

Rotation Invariant Point Cloud Classification: Where Local Geometry Meets Global Topology

Chen Zhao¹, Jiaqi Yang^{2,3}, Xin Xiong¹, Angfan Zhu¹, Zhiguo Cao^{*1}, and Xin Li⁴

¹School of Artificial Intelligence and Automation, Huazhong University of Science and Technology

²School of Computer Science, Northwestern Polytechnical University

³The National Engineering Laboratory for Integrated Aero-Space-Ground-Ocean Big Data Application Technology

⁴Lane Department of Computer Science and Electrical Engineering, West Virginia University

Abstract

Point cloud analysis is a basic task in 3D computer vision, which attracts increasing research attention. Most previous works develop experiments on synthetic datasets where the data is well-aligned. However, the data is prone to being unaligned in the real world, which contains SO_3 rotations. In this context, most existing works are ineffective due to the sensitivity of coordinate changes. For this reason, we address the issue of rotation by presenting a combination of global and local representations which are invariant to rotation. Moreover, we integrate the combination into a two-branch network where the highly dimensional features are hierarchically extracted. Compared with previous rotation-invariant works, the proposed representations effectively consider both global and local information. Extensive experiments have demonstrated that our method achieves state-of-the-art performance on the rotation-augmented version of ModelNet40, ShapeNet, and ScanObjectNN (real-world dataset).

1. Introduction

Recently, 3D computer vision has been playing a pivotal role in many applications, -e.g., autonomous driving [15, 21, 35], augmented reality [1], and robotics [7, 2]. Massive attention has been paid to point cloud which is a basic type of 3D data representation. As a pioneer of deep learning method towards point cloud analysis, PointNet [22] employs MLP to extract feature from raw 3D coordinates, which has been extensively following. Most previous works are evaluated on synthetic datasets, -i.e., Model-

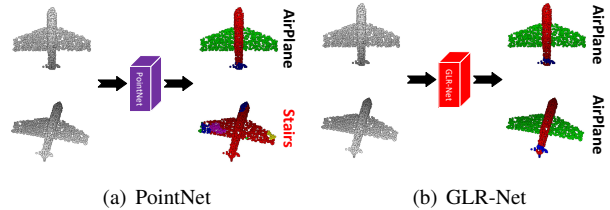


Figure 1. Superiority of our work compared with PointNet from the perspective of rotation invariance. The segmentation and classification results generated by PointNet (a) are considerably affected by rotation changes, while the results of our method (b) are identical facing the challenge of rotation.

Net40 [33] and ShapeNet [36], where the point-cloud models are well aligned. Nevertheless, it is non-trivial to get well aligned point clouds in the real world, where rotation is inevitable. Specifically, the pose of point-cloud models is arbitrary which includes translation and SO_3 rotation. PointNet and its modified versions fail in this case because of the variation of coordinates caused by transformations. As shown in Fig. 1(a), the classification and segmentation results are significantly confused by the rotation transformation. Considering that the issue of translation can be easily addressed by centering the point-cloud models, some attempts have been developed concentrating on rotation robustness. An intuitive solution is augmenting the training data using arbitrary rotation. However, the augmentation is unable to cover all SO_3 rotations with 3 degrees of freedom due to the limited capacity. An alternative way is using Spherical Fourier Transform to achieve rotation equivariance [8, 4], which still needs some extra process such as max pooling to achieve rotation invariance, and the loss of information is inevitable during the projection.

*Corresponding author

The issue of rotation sensitivity is able to be boiled down to changes of input coordinates. Inspired by this discovery, we expect to transform the raw coordinates into some rotation-invariant representations as the input of the network, which can achieve intrinsically invariant to the rotation. Although some rotation-invariant representations have been designed [37, 3], existing methods focus on utilizing distance and angles in some local regions, lacking the constrain of global information, which leads to the limited distinctiveness. In this regard, we present a simple yet effective solution to tackle the rotation problem, which combines global and local rotation-invariant features. Specifically, in the aspect of local representations, we extend Darboux feature [25] into a more distinctive feature space, where the relative locations are distinguished by measuring the distance and difference of local coordinate systems between the query point and its neighbors. For global representations, we estimate a global coordinate system on the down sampling point-cloud model employing singular value decomposition [10]. Subsequently, the original points are able to be projected into the estimated coordinate system which is invariant to the rotation.

Additionally, in order to extract highly dimensional feature from our presented representations, we propose a two-brunch network where the global and local representations are individually processed. The group convolution layer is designed as a basic module, which hierarchically extracts and aggregates features. As illustrated in Fig.1, the presented method is fully invariant to the rotation in classification and segmentation tasks. Extensive experiments are developed in both synthetic datasets, -i.e., ModelNet40 [33] and ShapeNet [36], and the real-world dataset, -i.e., ScanObjectNN [29], which show that our method achieves state-of-the-art performance for classification and segmentation tasks on rotation-augmented benchmark.

In a nutshell, Our major contributions are summarized as follows:

- We present a combination of global and local representations which are intrinsically invariant to rotation changes.
- We propose a two-brunch network¹ which employs group convolutions to hierarchically extract and aggregate features.
- Our method achieves state-of-the-art performance on comprehensive evaluation benchmarks which contain SO_3 rotation in both synthetic and real-world data.

¹The code will be available at <https://github.com/sailor-z/GLR-Net>

2. Related Work

Spatial transformations. To alleviate rotation issue, a straightforward way is augmenting training data using arbitrary rotation transformations [22, 22]. However, there are three degrees of freedom in the real world, -i.e., pitch, yaw, and roll, and each freedom ranges from 0 to 360, which leads to innumerable SO_3 rotations. Consequently, it is impractical to cover all kinds of rotations in the limited capacity. In order to improve the robustness to rotation in a more efficient way, an alternative attempt suggests to employ deep learning methods to immediately learn some spatial transformations [22]. Specifically, T-Net is used in PointNet to regress a 3×3 spatial transformation and a 64×64 highly dimensional transformation, with the expectation of transforming the point clouds into a canonical coordinate system. Nevertheless, the learned transformations are still vulnerable against the nuisance of rotation, because the regression procedure lacks a theoretical support from the perspective of rotation invariance.

Rotation equivariance convolutions. Inspired by the tremendous process of convolution networks in 2D computer vision, numerous works have been developed to bridge the success of convolutions from images to point clouds [34, 17, 32]. However, most previous works are sensitive to rotation, without taking the rotation invariance into account. In this regard, some efforts have been developed, which utilize spherical convolutions to achieve rotation equivariance [8, 4, 18]. First, the 3D mesh or voxel models are projected into spheres, translating the xyz coordinates into $\alpha\beta$ angles. Second, a series of spherical convolutions are carried out on the spheres to generate a set of feature maps, accomplished by Fourier Transform. Third, Inverse Fourier Transform is employed to recover the angles. However, note that the equivariance means the output and input vary equally, which is not intrinsically invariant to rotation. The global process such as global max pooling is crucial in order to achieve the rotation invariance. Additionally, the loss of information is inevitable during the generation of mesh/voxel, the transformation and inverse transformation, which leads to the limited performance.

Rotation invariance representations. For the sake of interior rotation invariance, some approaches attempt to transform the raw point clouds into rotation invariance representations, where distance and angles are the most widely used features. Specifically, Deng et al. [5] proposed a 4D point pair feature (PPF) for the task of rotation-invariant descriptors, which utilized the distance and angles between the central reference and neighbors in a local patch, combining the information of normal vectors. For the tasks of classification and segmentation, Chen et al. [3] integrated distance, angles, \sin , and \cos features in local k -NN graphs into a

cluster network. Zhang et al. [37] combined distance and angle features in local graphs and ones in reference points generated by down sampling. Nevertheless, all previous works concentrated on local features, -i.e., relative distance and angles in local graphs, lacking directions of effective global features. It makes sense that only employs local information in the field of local descriptors, while the local features are prone to being ambiguous for the tasks of classification and segmentation. For instance, the relative distance and angles tend to be similar among different regions in the same plane of a desk. In this regard, we present a combination of global and local rotation-invariant representations, filling in the gap of global constrains. The details will be introduced in the following section.

3. Method

3.1. Problem Statement

Our method directly processes raw point clouds as input, which are represented as a set of 3D points $\mathcal{P} \in \mathbb{R}^{N \times 3}$, -i.e., $\mathcal{P} = \{\mathbf{p}_i | i = 1, 2, \dots, n\}$ with $\mathbf{p}_i = (x_i, y_i, z_i)$. The normal vector of each point is also utilized which is indicated by $\mathbf{n}_i = (n_x^i, n_y^i, n_z^i)$. The rotation issue is formulated by transforming \mathcal{P} through a 3×3 orthogonal matrix $\mathbf{R} \in SO(3)$ ($\det(\mathbf{R}) = 1$), which contains three degrees of freedom, -i.e., $\alpha \in [0, 2\pi], \beta \in [0, \pi]$, and $\gamma \in [0, 2\pi]$. The task of rotation invariance is able to be boiled down to

$$\mathcal{F}(R(\mathcal{P})) = \mathcal{F}(\mathcal{P}), \quad (1)$$

where $\mathcal{F} : \mathbb{R}^{N \times 3} \rightarrow \mathbb{R}^{N \times D}$ is the function that generates the presented representations from raw points.

For the classification task with s classes, the output of our approach are s scores where the maximum score is expected to correspond to the correct class label. For semantic segmentation task, our method outputs a $N \times m$ score map, which indicates the scores of m categories for all points. Both the two tasks are supposed to be invariant to the rotation changes.

3.2. Local Branch

As aforementioned, local features have been proved to be critical for the point-cloud classification and segmentation [34, 17, 32]. To this end, we also design a local branch to extract local patterns in graph-based structures. Intuitively, the distance and angle are two kinds of rotation-invariant features, while the core issue is how to utilize these features in an effective way. Inspired by the classical Darboux [25], we dig out local geometrical features by estimating the relative relationships of local coordinate systems between the central point and its neighbors.

The representation is illustrated in Fig. 3. First, for a query point \mathbf{p}_1 , a local graph is generated by k-nearest searching, where \mathbf{p}_2 is one of the neighbors. Second, the

Euclidean distance $\|\vec{d}\|$ is calculated to indicate the local intensity around \mathbf{p}_1 , where \vec{d} is the relative vector between \mathbf{p}_1 and \mathbf{p}_2 , -i.e., $\vec{d} = \mathbf{p}_2 - \mathbf{p}_1$. Third, the relationship between the local coordinate systems centred in \mathbf{p}_1 and \mathbf{p}_2 is recovered. Note that normal vectors (\vec{n}_1, \vec{n}_2) are required to generate local coordinate systems. Specifically, in order to determine three orthogonal vectors $(\vec{n}_1, \vec{u}_1, \vec{v}_1)$ as an example, we leverage cross product to estimate \vec{u}_1 and \vec{v}_1 as

$$\vec{u}_1 = \vec{d} \times \vec{n}_1, \quad (2)$$

$$\vec{v}_1 = \vec{u}_1 \times \vec{n}_1. \quad (3)$$

Subsequently, the relationship is represented by $\{\theta_1, \theta_2, \theta_3, \theta_4, \theta_5, \theta_6, \theta_7\}$, which respectively indicates the angle between (\vec{d}, \vec{n}_1) , (\vec{d}, \vec{n}_2) , (\vec{n}_1, \vec{n}_2) , (\vec{u}_1, \vec{u}_2) , (\vec{v}_1, \vec{v}_2) , (\vec{u}_1, \vec{v}_2) , (\vec{v}_1, \vec{u}_2) . The angle $(\theta_1$ as an example) is calculated as

$$\theta_1 = \frac{\vec{d} \cdot \vec{n}_1}{\|\vec{d}\| \|\vec{n}_1\|} \quad (4)$$

Note that θ_6 and θ_7 are employed to alleviate the ambiguity. Given k neighbors for a query point \mathbf{p} , the generated representation is a $k \times 8$ feature map which fully mines the local pattern around \mathbf{p} .

3.3. Global Branch

Although local information has been extensively employed in rotation-invariant point cloud analysis, the extraction of global information is still an intractable issue. As mentioned in [37], the limited accuracy of their method is due to the lack of original point coordinates, which reflect the absolute locations in a global coordinate system. The classification result significantly increases when they replace the presented features with raw 3D coordinates, while the approach is no longer invariant to rotation. This observation is reasonable because the local features represent relative relationships which are inevitable to be ambiguous in some cases. For instance, for some points located on a flat plane of a table, the local representations, -i.e., distance and angles, tend to be similar among different neighbors. To this end, we design a global branch which contains a global feature extraction module, taking into account of rotation invariance.

An intuitive solution to extract global features is establishing a global coordinate system leveraging singular value decomposition to dig out three main directions which are equivariant to rotation changes. Nevertheless, it is time consuming that uses SVD in the original point-cloud model which may contain thousands of points, and SVD is also sensitive to the data missing. In order to achieve an efficient and robust solution, as shown in Fig. 4, we establish a down-sampling subset of the original model $\mathcal{P}' \subset \mathcal{P}$, which contains much fewer points, while remains the major geomet-

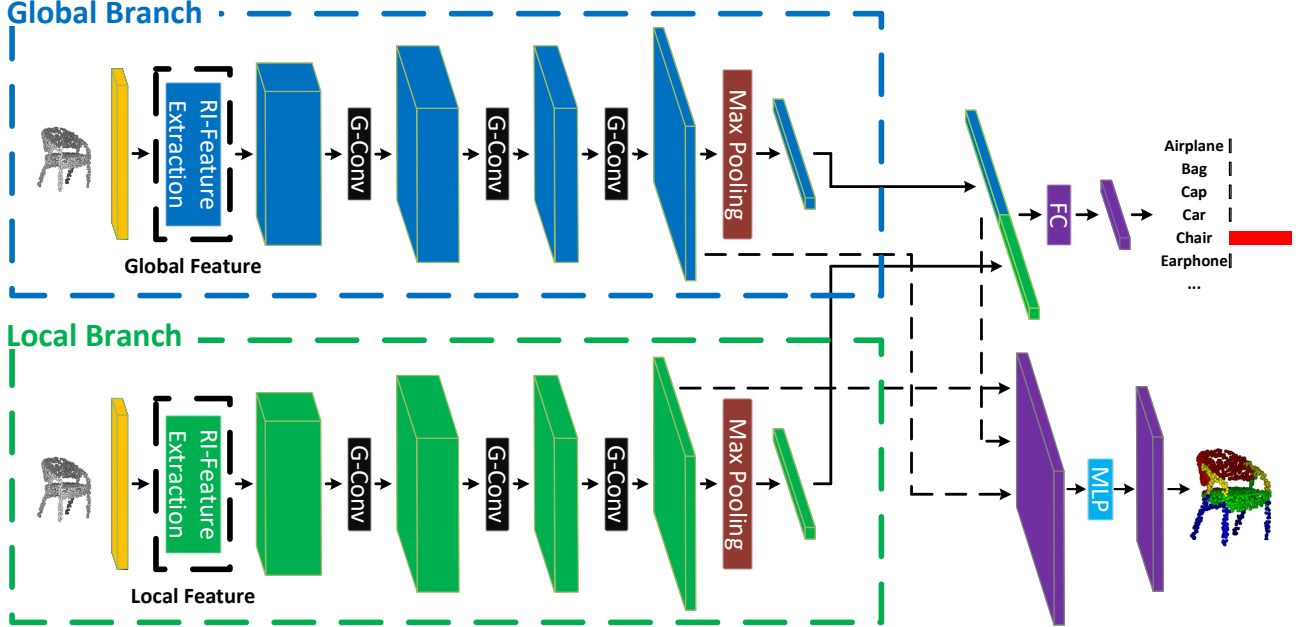


Figure 2. **Network architecture.** The architecture includes two branches which individually process 3D points $\mathcal{P} \in \mathbb{R}^{N \times 3}$. The global and local rotation-invariant features are individually extracted in two branches. The highly dimensional features are then hierarchically extracted and aggregated by a series of group convolutions (G-Conv). The feature embedding is generated by max pooling and concatenating two feature maps output by two branches, which is further processed by fully connected layers (FC) and multi-layer perceptrons (MLP) for classification and segmentation, respectively.

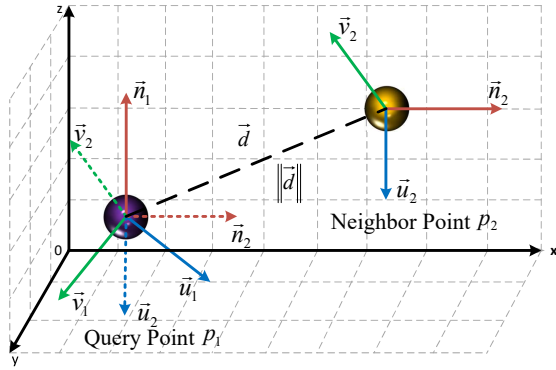


Figure 3. RI-feature extraction in the local branch. For a query point \mathbf{p}_1 , the relative location of its neighbor \mathbf{p}_2 is determined by estimating the Euclidean distance $\|\vec{d}\|$ of $\vec{d} = \mathbf{p}_2 - \mathbf{p}_1$ and relationships of local coordinate systems $(\vec{n}_1, \vec{u}_1, \vec{v}_1)$ and $(\vec{n}_2, \vec{u}_2, \vec{v}_2)$, where (\vec{n}_1, \vec{n}_2) are the normal vectors of $(\mathbf{p}_1, \mathbf{p}_2)$, and other axes are located by the cross product.

rical structure, -i.e., skeleton. The down-sampling procedure is implemented by farthest point sampling in this paper which is able to increase the robustness against nuisances.

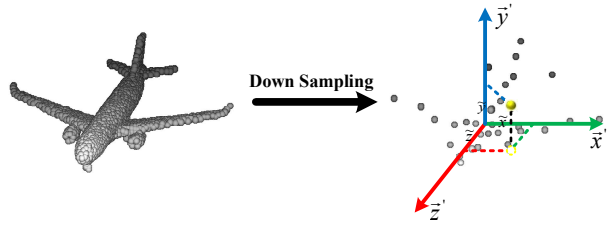


Figure 4. RI-feature extraction in the global branch. A global coordinate system is generated on the down-sampling model, using singular value decomposition. Points in the original model are projected into the generated coordinate system, where the coordinates are invariant to rotation changes.

SVD is then carried out on \mathcal{P}' formulated as

$$\mathbf{U}\Sigma\mathbf{V}^T = \mathbf{P}', \quad (5)$$

where \mathbf{V} contains the generated three orthogonal axes. The invariance against rotation is achieved by transforming points of the original model into the established global coordinate system as

$$\hat{\mathbf{P}} = \mathbf{P} \cdot \mathbf{V}. \quad (6)$$

3.4. Group Convolution

For purpose of extracting highly dimensional features from the presented representations, we integrate the RI-feature extraction module into a deep learning framework.

Inspired by the success of deep learning in 2D computer vision [6, 27, 12], massive efforts have been widely carried out for point cloud analysis [22], which mainly employ MLP as a basic feature extraction module. Further, to aggregate local information which has been proved to be critical in 2D convolution neural networks, some approaches such as graph-based convolutions [11, 30, 31] and local max pooling have been developed. However, the previous works include interior drawbacks. For instance, graph-based methods are space consuming and local max pooling carried out after MLP which still individually processes each point leads to the inevitable loss of information. To this end, we design a series of group convolution layers which are able to hierarchically extract and aggregate features in an efficient way. Note that our framework is intrinsically invariant to rotation changes owing to the rotation-invariant representations.

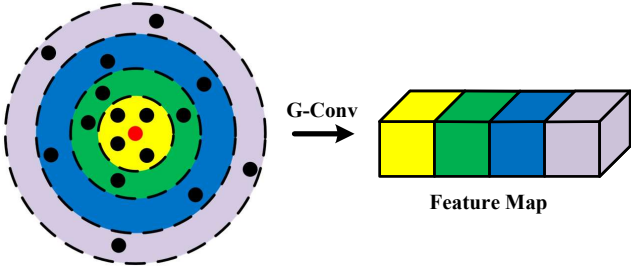


Figure 5. **Group Convolution.** The red dot indicates the central point and the other dots represent its neighbors. The neighbors are distributed into several groups (shown by different colors) based on the distance from the central point. Features in a group are aggregated into a block by the group convolution (G-Conv). The output feature map is then established by concatenating all blocks generated from different groups.

As shown in Fig. 5, for a central point $s \in \mathbb{R}^c$ (red dot), where c represents the feature dimension, a graph $\mathbf{A} \in \mathbb{R}^{k \times c}$ is established by k -nearest searching in the xyz space. The neighbors (black dots) are distributed into several groups $\{\mathcal{G}_1, \mathcal{G}_2, \dots, \mathcal{G}_n\}$ according to the Euclidean distance from the central point, which transforms the unordered points into a sorted format. The group convolution is able to be conducted on the groups as

$$\mathbf{F}_j = \sum_{i=1}^{\lfloor k/n \rfloor} \omega s_i, \quad (7)$$

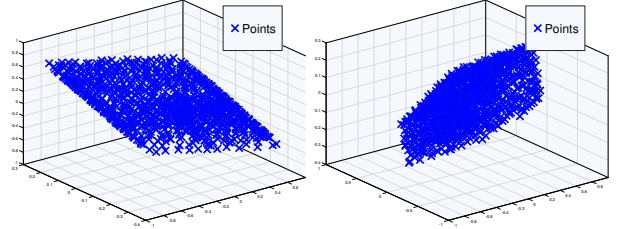
where ω is a set of learning weights which are shared among different groups, and \mathbf{F}_j is the aggregated feature block of \mathcal{G}_j . The feature map $\mathbf{F} \in \mathbb{R}^{n \times h}$ is output by concatenating all feature blocks as

$$\mathbf{F} = \text{cat}(\mathbf{F}_1, \mathbf{F}_2, \dots, \mathbf{F}_n). \quad (8)$$

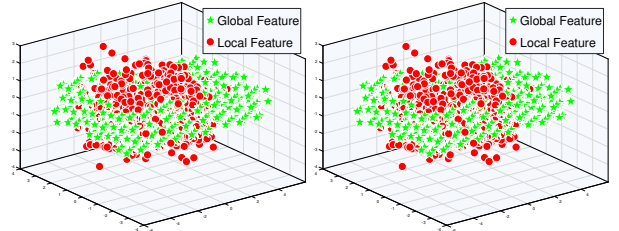
Instead of using the combination of MLP and local max pooling which is accountable for the loss of information, we

employ a set of group convolutions to hierarchically aggregate the input $N \times k \times C_{in}$ representation into a $N \times 1 \times C_{out}$ feature map, which intensively digs out the effective local information.

3.5. Rotation-Invariant Analysis



(a) Raw point locations with different orientations



(b) Rotation-invariant representations

Figure 6. Comparison of the robustness against rotation between (a) raw point locations and (b) presented rotation-invariant representations which are visualized in 3D space by *t-sne* [19]. Under two different orientations, the raw coordinates of 3D points are significantly changed, while all the locations of our global and local representations are invariant.

As demonstrated in Fig. 6, we visualize the extracted global and local representations in the 3D space using *t-sne* [19]. Compared with raw point locations in Fig. 6 (a) which are sensitive to orientation changes, the projected locations of our representations in Fig. 6 (b) are identical facing the challenge of rotation, which intrinsically guarantees the robustness against rotation for the subsequent learning process.

The theoretical demonstration is also introduced as follows.

Distance. Assuming (d, d') is the $L2$ norm of $(\mathbf{p}, \mathbf{p}')$, where $\mathbf{p}' = \mathbf{p}\mathbf{R}$, the invariance against rotation is able to be proved as

$$d' = \|\mathbf{p}\mathbf{R}\| = \mathbf{p}\mathbf{R}\mathbf{R}^T\mathbf{p} = d. \quad (9)$$

Angle. Supposing $(\theta_{ij}, \theta'_{ij})$ are the angles between $(\mathbf{p}_i, \mathbf{p}_j)$ and $(\mathbf{p}'_i, \mathbf{p}'_j)$, the equivalence is formulated as

$$\theta'_{ij} = \frac{\mathbf{p}'_i \mathbf{p}'_j{}^T}{\|\mathbf{p}'_i\| \|\mathbf{p}'_j\|} = \frac{\mathbf{p}_i \mathbf{R} \mathbf{R}^T \mathbf{p}_j}{\|\mathbf{p}_i\| \|\mathbf{p}_j\|} = \theta_{ij}. \quad (10)$$

Singular Value Decomposition. We define two point clouds as \mathbf{P} and \mathbf{P}' ($\mathbf{P}, \mathbf{P}' \in \mathbb{R}^{N \times 3}$) with $\mathbf{P}' = \mathbf{P}\mathbf{R}$. Singular value decomposition is respectively performed as

$$\mathbf{U}\Sigma\mathbf{V}^T = \mathbf{P}, \quad (11)$$

$$\mathbf{U}'\Sigma\mathbf{V}'^T = \mathbf{P}', \quad (12)$$

so the relationship between \mathbf{V} and \mathbf{V}' is able to be derived as $\mathbf{V}' = \mathbf{R}^T\mathbf{V}$. The invariance of point locations transformed by \mathbf{V} is then shown as

$$\mathbf{P}'\mathbf{V}' = \mathbf{P}\mathbf{R}\mathbf{R}^T\mathbf{V} = \mathbf{P}\mathbf{V}, \quad (13)$$

4. Experiments

In this section, we develop experiments on three datasets designed for different tasks, -i.e., ModelNet40 [33] (Synthetic shape classification), ScanObjectNN [29] (Real world shape classification), and ShapeNet [36] (Part segmentation). Ablation study is also performed to evaluate the effectiveness of our network design.

4.1. Implementation Details

For local graph generation, we use k -nearest searching to find out 32 neighbors for each central point. In global branch, we down sample the original model into 32 points utilizing farthest point sampling. For group convolutions which are individual between two branches, the dimensions (64, 128, 512, 1024) are employed. Each group convolution is followed by Batch Normalization [13] and LeakyReLU [9]. We use three fully connected layers (512, 256, N_{cls}) to predict classification results, and three layers of MLP (512, 256, N_{seg}) to generate segmentation results, where N_{cls} and N_{seg} indicate the number of candidate labels.

4.2. Synthetic Shape Classification

We evaluate our method on ModelNet40 which has been extensively used for synthetic shape classification [16, 14]. ModelNet40 includes 12311 CAD models from 40 categories that are split into 9843 for training and 2468 for testing. We randomly sample 1024 points from each model. These points are then centralized and normalized into a unit sphere.

We divide previous works into two categories, -i.e., rotation-sensitive method and rotation-robust method. The experiments are performed in three different cases, -i.e., raw training data and testing data, raw training data and 3D rotation-augmented testing data, and 3D rotation-augmented training data and testing data, which are respectively indicated by z/z , $z/SO3$, and $SO3/SO3$. Table 1

lists the experimental results. First, In the case of z/z , our method (GLR-Net) surpasses the other rotation-robust methods. Compared with Spherical-CNN and a^3S -CNN where mesh information is necessary, our method achieves superior performance even though we use raw points as input, which verifies our framework is more effective than spherical solutions. For ClusterNet and Riconv which also propose some local rotation-invariant representations, the lack of global information leads to inferior performance compared with our method. Second, in the situations of $z/SO3$ and $SO3/SO3$, the results of GLR-Net are almost identical, exceeding other ones by a large margin, while the results of rotation-sensitive algorithms considerably decline. The previous state-of-the-art approach (DGCNN) is vulnerable in $z/SO3$, which only gets a 20.6% accuracy. The performance is still unsatisfactory (81.1%) in $SO3/SO3$, even though the training data is augmented by 3D rotations. These phenomenons show that it is crucial to take into account of rotation robustness for the applications in the real world.

4.3. Real World Shape Classification

For purpose of analysing the limitation of our method, we estimate the confusion matrix which is shown in Fig. 7 (a). An unexpected discovery is observed that ModelNet40 contains interior ambiguity. Specifically, as illustrated in Fig. 7 (a), the most two confusing categories are flower pot and plant, so we show the models belong to these categories in Fig. 7 (b), where both two models include similar plants and pots. They are ambiguous that can not be explicitly classified even by human beings. Additionally, considering

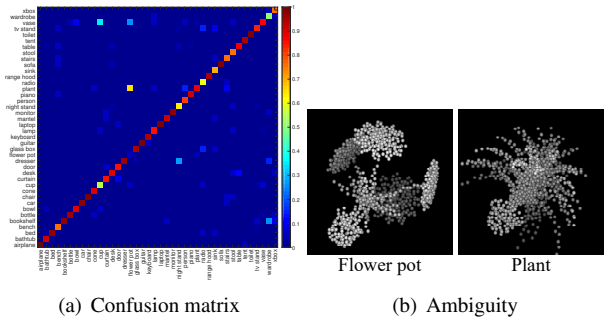


Figure 7. Analysis for the limitation of ModelNet40. The confusion matrix (a) is estimated which shows the classification result of all 40 candidate labels. The flower pot and plant are the most confusing categories which are illustrated in (b). Both two models include similar plants and pots, which demonstrates ModelNet40 contains the interior ambiguity where some shape models can not be explicitly classified even by human beings.

that the objects in ModelNet40 are man-made CAD models, which are thus well-aligned and noise-free, there is a significant gap between the synthetic data and real-world data which tends to include different oriented objects and

Rotation-sensitive Method	input	# views	z/z (%)	$z/SO3$ (%)	$SO3/SO3$ (%)
VoxNet [20]	volume	12	83.0	-	73.0
Subvolume [23]	volume	20	89.5	45.5	85.0
MVCNN [28]	image	80	90.2	81.5	86.0
PointNet [22]	point	1	89.2	16.4	75.5
PointNet++ [24]	point	1	91.8	18.4	77.4
PointCNN [17]	point	1	91.3	41.2	84.5
DGCNN [32]	point	1	92.2	20.6	81.1
Rotation-robust Method	input	# views	z/z (%)	$z/SO3$ (%)	$SO3/SO3$ (%)
Spherical-CNN [8]	mesh	1	88.9	76.7	86.9
a^3 S-CNN [18]	mesh	1	89.6	87.9	88.7
ClusterNet [3]	point	1	87.1	87.1	87.1
Riconv [37]	point	1	86.5	86.4	86.4
GLR-Net	point	1	90.2	90.2	89.7

Table 1. Synthetic shape classification results on ModelNet40. The evaluated algorithms are divided into rotation-sensitive method and rotation-robust method. The experiments are performed in three situations based on different combinations of training data and testing data. z and $SO3$ are respectively represent raw data and 3D rotation-augmented data. The metric is classification accuracy and the best result is rendered in bold.

various nuisances, -e.g., missing data, occlusion, and non-uniform density. In order to evaluate the performance of shape classification in the real world and the robustness against noises in a reliable way, we perform experiments on ScanObjectNN [29] which is collected in the real-world indoor scenes on the one hand and declares to discard ambiguous objects on the other hand. This dataset includes 2902 objects that are categorized into 15 categories, taking into account of one freedom rotation, translation, missing data, background noise, occlusion, and non-uniform density. Some examples in this dataset are shown in Fig. 8.



Figure 8. Object examples in ScanObjectNN.

We develop the experiments on the easiest part OBJ_BG without rotation, translation, and scaling, and the hardest part PB_T50_RS which contains 50% bounding box translation, rotation around the gravity axis, and random scaling. The evaluated results are shown in Table 2. Our method achieves the best performance compared with previous works, which indicates that GLR-Net is not only invariant to rotation, but also robust to common nuisances. Consequently, it is promising to utilize our method for the classification task in the real world. However, the performances of GLR-Net considerably decline compared with the ones in Table 1, which suggests that there is still a large room for further improvement from the perspectives of robustness and generalization.

Method	OBJ_BG		PB_T50_RS	
	$z/SO3$	$SO3/SO3$	$z/SO3$	$SO3/SO3$
PointNet [22]	16.7	54.7	17.1	42.2
PointNet++ [24]	15.0	47.4	15.8	60.1
SpiderCNN [34]	17.6	58.9	15.4	46.4
DGCNN [32]	17.7	71.8	16.1	63.4
PointCNN [17]	14.6	63.7	14.9	51.8
Riconv [37]	78.4	78.1	67.9	68.3
GLR-Net	79.0	78.8	68.2	68.6

Table 2. Real world shape classification results on ScanObjectNN. Two parts, -i.e., OBJ_BG and PB_T50_RS are considered. OBJ_BG contains objects and backgrounds without rotation, translation, and scaling, while PB_T50_RS takes into account of 50% bounding box translation, rotation around the gravity axis, and random scaling. The performance is measured by classification accuracy.

4.4. Part Segmentation

Given a point-cloud model, the target of segmentation is accurately predicting per-point labels. Compared with the shape classification, segmentation is a more challenging task which requires the capacity of capturing fine-grained patterns. Consequently, we extend our experiments on ShapeNet [36] which is a widely used dataset for part segmentation evaluation. We use a part of ShapeNet that includes 16881 3D models from 16 kinds of objects with 50 part categories. Overall average category mIoU (Cat. mIoU) [26] is utilized to measure the segmentation performance, which is calculated by immediately averaging the results over 16 categories.

The general results are reported in Table 5, and the specific results are listed in Table 3 and Table 4. In the situation without rotation (z/z), our approach considerably sur-

Method	aero	bag	cap	car	chair	earph.	guitar	knife	lamp	laptop	motor	mug	pistol	rocket	skate	table
#shapes	2690	76	55	898	3758	69	787	392	1547	451	202	184	283	66	152	5271
PointNet	40.4	48.1	46.3	24.5	45.1	39.4	29.2	42.6	52.7	36.7	21.2	55.0	29.7	26.6	32.1	35.8
PointNet++	51.3	66.0	50.8	25.2	66.7	27.7	29.7	65.6	59.7	70.1	17.2	67.3	49.9	23.4	43.8	57.6
PointCNN	21.8	52.0	52.1	23.6	29.4	18.2	40.7	36.9	51.1	33.1	18.9	48.0	23.0	27.7	38.6	39.9
DGCNN	37.0	50.2	38.5	24.1	43.9	32.3	23.7	48.6	54.8	28.7	17.8	74.4	25.2	24.1	43.1	32.3
Riconv	79.1	76.4	73.9	69.1	87.0	68.6	89.0	80.0	75.6	75.3	54.1	89.5	74.5	52.9	65.1	77.1
Ours	81.0	76.9	79.5	73.4	86.0	67.5	89.4	85.6	83.1	83.1	62.7	91.3	76.0	61.4	78.2	78.9

Table 3. Specific per-class average mIoU in the case of $z/SO3$.

Method	aero	bag	cap	car	chair	earph.	guitar	knife	lamp	laptop	motor	mug	pistol	rocket	skate	table
PointNet	81.6	68.7	74.0	70.3	87.6	68.5	88.9	80.0	74.9	83.6	56.5	77.6	75.2	53.9	69.4	79.9
PointNet++	79.5	71.6	87.7	70.7	88.8	64.9	88.8	78.1	79.2	94.9	54.3	92.0	76.4	50.3	68.4	81.0
PointCNN	78.0	80.1	78.2	68.2	81.2	70.2	82.0	70.6	68.9	80.8	48.6	77.3	63.2	50.6	63.2	82.0
DGCNN	77.7	71.8	77.7	55.2	87.3	68.7	88.7	85.5	81.8	81.3	36.2	86.0	77.3	51.6	65.3	80.2
Riconv	79.2	73.1	75.5	68.8	86.8	68.9	89.0	79.8	76.4	77.5	57.0	89.3	70.9	48.5	66.6	77.8
Ours	81.2	77.3	79.1	72.5	86.0	71.1	88.7	84.8	82.4	84.3	59.2	91.6	75.8	62.1	77.8	79.1

Table 4. Specific per-class average mIoU in the case of $SO3/SO3$.

Method	z/z (%)	$z/SO3$ (%)	$SO3/SO3$ (%)
PointNet	80.4	37.8	74.4
PointNet++	81.9	48.2	76.7
PointCNN	84.6	34.7	71.4
DGCNN	82.3	37.4	73.3
SpiderCNN	82.4	42.9	72.3
Riconv	74.6	74.2	73.7
GLR-Net	78.4	78.4	78.3

Table 5. Overall part segmentation results on ShapeNet. The metric is overall average category mIoU (Cat. mIoU) estimated by averaging the results over 16 categories.

passes the previous rotation-invariant algorithm (Riconv); In the case of 3D rotations ($z/SO3$ and $SO3/SO3$), GLR-Net achieves consistent performance, significantly exceeding other algorithms, which empirically confirms that GLR-Net makes a well trade-off between rotation invariance and Cat. mIoU.

4.5. Evaluations of Network Design

In order to further verify the effectiveness of our two-branch network design, we perform an ablation study. Specifically, we separate the global branch and local branch and individually employ each branch to train the classification network on ModelNet40.

As reported in Table 6, considerable decline occurs when the branch is individually used during the training step. It is confirmed that the combination of global and local representations is a promising solution to increase the distinctiveness in the embedded feature space. The two branches play complementary roles that reasonably take into account

of considerations from two different views, -i.e., global observation and local fine-grained patterns.

Global Branch	Local Branch	Acc. (%)
yes	-	87.4
-	yes	85.3
yes	yes	90.2

Table 6. Ablation study on ModelNet40.

4.6. Limitation

Although our method achieves state-of-the-art performances, the limitation is still can not be ignored. During the RI-feature extraction in global branch, the original model is projected into a global coordinate system estimated by SVD, which leads to various orientations among different models. Considering that the objects in existing datasets are well-aligned, the various orientations reduce the underlying consistence among the objects from the same category, which causes the loss of performance. However, due to the $SO3$ rotations in the real world, it is impractical to obtain well-aligned instances in practical applications. Our method still shows a promising prospect for the classification and segmentation tasks in the real world.

5. Conclusion

We have presented a combination of global and local representations which are intrinsically invariant to $SO3$ rotations. For further highly dimensional feature extraction, we integrate the representations into a two-branch network where a series of group convolutions are designed to hierarchically extract and aggregate features. Both theoretical and

empirical proofs for the invariance against rotations are provided. Experiments also demonstrate the superiority of our two-branch network design. Our method shows a promising prospect for the real-world applications.

References

- [1] E. Alexiou, E. Upenik, and T. Ebrahimi. Towards subjective quality assessment of point cloud imaging in augmented reality. In *2017 IEEE 19th International Workshop on Multimedia Signal Processing (MMSP)*, pages 1–6. IEEE, 2017.
- [2] T. Bailey and H. Durrant-Whyte. Simultaneous localization and mapping (slam): Part ii. *IEEE robotics & automation magazine*, 13(3):108–117, 2006.
- [3] C. Chen, G. Li, R. Xu, T. Chen, M. Wang, and L. Lin. Clusternet: Deep hierarchical cluster network with rigorously rotation-invariant representation for point cloud analysis. In *Proceedings of the IEEE Conference on Computer Vision and Pattern Recognition*, pages 4994–5002, 2019.
- [4] T. S. Cohen, M. Geiger, J. Köhler, and M. Welling. Spherical cnns. In *International Conference on Learning Representations*, 2018.
- [5] H. Deng, T. Birdal, and S. Ilic. Ppf-foldnet: Unsupervised learning of rotation invariant 3d local descriptors. In *Proceedings of the European Conference on Computer Vision*, pages 602–618, 2018.
- [6] J. Deng, W. Dong, R. Socher, L.-J. Li, K. Li, and L. Fei-Fei. Imagenet: A large-scale hierarchical image database. In *Proceedings of the IEEE Conference on Computer Vision and Pattern Recognition*, pages 248–255. Ieee, 2009.
- [7] H. Durrant-Whyte and T. Bailey. Simultaneous localization and mapping: part i. *IEEE robotics & automation magazine*, 13(2):99–110, 2006.
- [8] C. Esteves, C. Allen-Blanchette, A. Makadia, and K. Daniilidis. Learning so (3) equivariant representations with spherical cnns. In *Proceedings of the European Conference on Computer Vision*, pages 52–68, 2018.
- [9] X. Glorot, A. Bordes, and Y. Bengio. Deep sparse rectifier neural networks. In *Proceedings of the International Conference on Artificial Intelligence and Statistics*, pages 315–323, 2011.
- [10] G. H. Golub and C. Reinsch. Singular value decomposition and least squares solutions. In *Linear Algebra*, pages 134–151. Springer, 1971.
- [11] L. Hansen, J. Diesel, and M. P. Heinrich. Multi-kernel diffusion cnns for graph-based learning on point clouds. In *Proceedings of the European Conference on Computer Vision*, pages 0–0, 2018.
- [12] K. He, X. Zhang, S. Ren, and J. Sun. Deep residual learning for image recognition. In *Proceedings of the IEEE Conference on Computer Vision and Pattern Recognition*, pages 770–778, 2016.
- [13] S. Ioffe and C. Szegedy. Batch normalization: Accelerating deep network training by reducing internal covariate shift. *arXiv preprint arXiv:1502.03167*, 2015.
- [14] M. Jiang, Y. Wu, T. Zhao, Z. Zhao, and C. Lu. Pointsift: A sift-like network module for 3d point cloud semantic segmentation. *arXiv preprint arXiv:1807.00652*, 2018.
- [15] B. Li, W. Ouyang, L. Sheng, X. Zeng, and X. Wang. Gs3d: An efficient 3d object detection framework for autonomous driving. In *Proceedings of the IEEE Conference on Computer Vision and Pattern Recognition*, pages 1019–1028, 2019.
- [16] J. Li, B. M. Chen, and G. Hee Lee. So-net: Self-organizing network for point cloud analysis. In *Proceedings of the IEEE Conference on Computer Vision and Pattern Recognition*, pages 9397–9406, 2018.
- [17] Y. Li, R. Bu, M. Sun, W. Wu, X. Di, and B. Chen. Pointcnn: Convolution on x-transformed points. In *Advances in Neural Information Processing Systems*, pages 820–830, 2018.
- [18] M. Liu, F. Yao, C. Choi, A. Sinha, and K. Ramani. Deep learning 3d shapes using alt-az anisotropic 2-sphere convolution. 2018.
- [19] L. v. d. Maaten and G. Hinton. Visualizing data using t-sne. *Journal of Machine Learning Research*, 9(Nov):2579–2605, 2008.
- [20] D. Maturana and S. Scherer. Voxnet: A 3d convolutional neural network for real-time object recognition. In *IEEE/RSJ International Conference on Intelligent Robots and Systems*, pages 922–928. IEEE, 2015.
- [21] G. P. Meyer, A. Laddha, E. Kee, C. Vallespi-Gonzalez, and C. K. Wellington. Lasernet: An efficient probabilistic 3d object detector for autonomous driving. In *Proceedings of the IEEE Conference on Computer Vision and Pattern Recognition*, pages 12677–12686, 2019.
- [22] C. R. Qi, H. Su, K. Mo, and L. J. Guibas. Pointnet: Deep learning on point sets for 3d classification and segmentation. In *Proceedings of the IEEE Conference on Computer Vision and Pattern Recognition*, pages 652–660, 2017.
- [23] C. R. Qi, H. Su, M. Nießner, A. Dai, M. Yan, and L. J. Guibas. Volumetric and multi-view cnns for object classification on 3d data. In *Proceedings of the IEEE Conference on Computer Vision and Pattern Recognition*, pages 5648–5656, 2016.
- [24] C. R. Qi, L. Yi, H. Su, and L. J. Guibas. Pointnet++: Deep hierarchical feature learning on point sets in a metric space. In *Advances in neural information processing systems*, pages 5099–5108, 2017.
- [25] R. B. Rusu, N. Blodow, Z. C. Marton, and M. Beetz. Aligning point cloud views using persistent feature histograms. In *2008 IEEE/RSJ International Conference on Intelligent Robots and Systems*, pages 3384–3391. IEEE, 2008.
- [26] Y. Shen, C. Feng, Y. Yang, and D. Tian. Mining point cloud local structures by kernel correlation and graph pooling. In *Proceedings of the IEEE Conference on Computer Vision and Pattern Recognition*, pages 4548–4557, 2018.
- [27] K. Simonyan and A. Zisserman. Very deep convolutional networks for large-scale image recognition. *arXiv preprint arXiv:1409.1556*, 2014.
- [28] H. Su, S. Maji, E. Kalogerakis, and E. Learned-Miller. Multi-view convolutional neural networks for 3d shape recognition. In *Proceedings of the IEEE International Conference on Computer Vision*, pages 945–953, 2015.
- [29] M. A. Uy, Q.-H. Pham, B.-S. Hua, D. T. Nguyen, and S.-K. Yeung. Revisiting point cloud classification: A new bench-

- mark dataset and classification model on real-world data. *arXiv preprint arXiv:1908.04616*, 2019.
- [30] D. Valsesia, G. Fracastoro, and E. Magli. Learning localized generative models for 3d point clouds via graph convolution. 2018.
- [31] C. Wang, B. Samari, and K. Siddiqi. Local spectral graph convolution for point set feature learning. In *Proceedings of the European Conference on Computer Vision*, pages 52–66, 2018.
- [32] Y. Wang, Y. Sun, Z. Liu, S. E. Sarma, M. M. Bronstein, and J. M. Solomon. Dynamic graph cnn for learning on point clouds. *ACM Transactions on Graphics*, 38(5):146, 2019.
- [33] Z. Wu, S. Song, A. Khosla, F. Yu, L. Zhang, X. Tang, and J. Xiao. 3d shapenets: A deep representation for volumetric shapes. In *Proceedings of the IEEE conference on computer vision and pattern recognition*, pages 1912–1920, 2015.
- [34] Y. Xu, T. Fan, M. Xu, L. Zeng, and Y. Qiao. Spidercnn: Deep learning on point sets with parameterized convolutional filters. In *Proceedings of the European Conference on Computer Vision*, pages 87–102, 2018.
- [35] Z. Yang, Y. Sun, S. Liu, X. Shen, and J. Jia. Ipod: Intensive point-based object detector for point cloud. *arXiv preprint arXiv:1812.05276*, 2018.
- [36] L. Yi, V. G. Kim, D. Ceylan, I. Shen, M. Yan, H. Su, C. Lu, Q. Huang, A. Sheffer, L. Guibas, et al. A scalable active framework for region annotation in 3d shape collections. *ACM Transactions on Graphics*, 35(6):210, 2016.
- [37] Z. Zhang, B.-S. Hua, D. W. Rosen, and S.-K. Yeung. Rotation invariant convolutions for 3d point clouds deep learning. *arXiv preprint arXiv:1908.06297*, 2019.